Received: 8 April 2020 | Revised: 21 September 2020 | Accepted: 1 October 2020

DOI: 10.1111/jnc.15210

ORIGINAL ARTICLE

Journal of Neurochemistry JNC The Official Journal of the International Society for Neurochemistry WILEY

SynaptoPAC, an optogenetic tool for induction of presynaptic plasticity

Silvia Oldani[1,2] | Laura Moreno-Velasquez[2] | Lukas Faiss[1,2] | Alexander Stumpf[2] | Christian Rosenmund[2] | Dietmar Schmitz[1,2,3,4,5] | Benjamin R. Rost[1]

[1]German Center for Neurodegenerative Diseases (DZNE), Berlin, Germany

[2]Charité – Universitätsmedizin Berlin, corporate member of Freie Universität Berlin and Humboldt-Universität zu Berlin, and Berlin Institute of Health, NeuroCure Cluster of Excellence, Berlin, Germany

[3]Max-Delbruck-Centrum (MDC) for Molecular Medicine in the Helmholtz Association, Berlin, Germany

[4]Bernstein Center for Computational Neuroscience, Berlin, Germany

[5]Einstein Center for Neurosciences Berlin, Berlin, Germany

Correspondence
Dietmar Schmitz and Benjamin R. Rost, German Center for Neurodegenerative Diseases (DZNE), 10117 Berlin, Germany.
Email: dietmar.schmitz@charite.de (or) benjamin.rost@dzne.de

Funding information
Deutsche Forschungsgemeinschaft, Grant/Award Number: 390688087, SPP 1926, SPP 1665, SFB 1315 and SFB 958

Read the Editorial Highlight for this article on page 270.

Abstract

Optogenetic manipulations have transformed neuroscience in recent years. While sophisticated tools now exist for controlling the firing patterns of neurons, it remains challenging to optogenetically define the plasticity state of individual synapses. A variety of synapses in the mammalian brain express presynaptic long-term potentiation (LTP) upon elevation of presynaptic cyclic adenosine monophosphate (cAMP), but the molecular expression mechanisms as well as the impact of presynaptic LTP on network activity and behavior are not fully understood. In order to establish optogenetic control of presynaptic cAMP levels and thereby presynaptic potentiation, we developed synaptoPAC, a presynaptically targeted version of the photoactivated adenylyl cyclase bPAC. In cultures of hippocampal granule cells of Wistar rats, activation of synaptoPAC with blue light increased action potential-evoked transmission, an effect not seen in hippocampal cultures of non-granule cells. In acute brain slices of C57BL/6N mice, synaptoPAC activation immediately triggered a strong presynaptic potentiation at mossy fiber synapses in CA3, but not at Schaffer collateral synapses in CA1. Following light-triggered potentiation, mossy fiber transmission decreased within 20 min, but remained enhanced still after 30 min. The optogenetic potentiation altered the short-term plasticity dynamics of release, reminiscent of presynaptic LTP. Our work establishes synaptoPAC as an optogenetic tool that enables acute light-controlled potentiation of transmitter release at specific synapses in the brain, facilitating studies of the role of presynaptic potentiation in network function and animal behavior in an unprecedented manner.

KEYWORDS

dentate gyrus, hippocampus, long-term potentiation, optogenetics, presynaptic plasticity

Abbreviations: ACSF, artificial cerebrospinal fluid; bPAC, *Beggiatoa* photoactivated adenylyl cyclase; cAMP, cyclic adenosine monophosphate; EPSC, excitatory postsynaptic current; fEPSP, field excitatory postsynaptic potential; mEPSC, miniature excitatory postsynaptic current; MF, mossy fiber; PPR, paired-pulse ratio; Pvr, vesicular release probability; synaptoPAC, synaptic photoactivated adenylyl cyclase.

1 | INTRODUCTION

Long-term plasticity of synaptic transmission is considered as the cellular basis of learning and memory (Takeuchi et al., 2014). Specific patterns of activity can lead to strengthening or weakening of synapses on timescales ranging from minutes to days, thereby shaping the functional connectivity of neuronal ensembles. While postsynaptic plasticity involves changes in the number of receptors (Herring & Nicoll, 2016), presynaptic plasticity alters the transmitter release probability or the number of release sites (Monday et al., 2018). At several synapses in the mammalian central nervous system, presynaptic long-term potentiation (LTP) is initiated by an increase in cyclic adenosine monophosphate (cAMP) produced by calcium-stimulated adenylyl cyclases in the presynaptic terminal (Castillo, 2012; Ferguson & Storm, 2004). This process was first described for hippocampal mossy fiber (MF) synapses in CA3 (Huang et al., 1994; Weisskopf et al., 1994; Zalutsky & Nicoll, 1990), and subsequently for several other synapses, for example, the synapses between cerebellar parallel fibers and Purkinje cells (Salin et al., 1996), hippocampal CA1 pyramidal neurons and subiculum burst-firing cells (Wozny et al., 2008), hippocampal mossy cells and granule cells (Hashimotodani et al., 2017), cortical afferents to the thalamus and the lateral amygdala (Castro-Alamancos & Calcagnotto, 1999; Fourcaudot et al., 2008; Huang & Kandel, 1998), and the inhibitory synapses between cerebellar stellate cells (Lachamp et al., 2009).

The mechanisms of presynaptic LTP were studied most extensively at MF-CA3 synapses, formed between the axons of dentate gyrus granule cells and the dendrites of CA3 pyramidal cells (Nicoll & Schmitz, 2005). Here, high-frequency electrical stimulation of axons elicits first a strong post-tetanic potentiation of transmitter release, which decays within tens of minutes and is followed by LTP expressed as long-lasting increase of transmission. Alternatively, direct pharmacological activation of adenylyl cyclases by forskolin or application of the cAMP analogue Sp-cAMPS induces a sustained presynaptic potentiation (Huang et al., 1994; Tong et al., 1996; Weisskopf et al., 1994). The increase of presynaptic cAMP activates protein kinase A (PKA) and the guanine nucleotide exchange factor EPAC2 (Fernandes et al., 2015; Weisskopf et al., 1994). Several presynaptic molecules, including RIM1α, Rab3A, Munc13-1, and synaptotagmin12, have been postulated as downstream targets of cAMP (Castillo et al., 1997, 2002; Kaeser-Woo et al., 2013; Yang & Calakos, 2011), but despite decades of research, the exact mechanisms of presynaptic long-term potentiation remain elusive.

Significance statement

SynaptoPAC is a novel optogenetic tool that allows increasing synaptic transmission by light-controlled induction of presynaptic plasticity.

Both electrical and pharmacological inductions of presynaptic potentiation are not cell-type-specific and difficult to implement in living animals. This lack of minimally invasive and cell-specific tools for controlling presynaptic short- and long-term potentiation is one of the reasons why the computational and behavioral relevance of presynaptic LTP is largely unclear (Monday et al., 2018). To fill this gap, here we establish an optogenetic tool for cell-type-specific manipulation of presynaptic plasticity directly at the axonal terminal. Optogenetic manipulations overcome many of the shortcomings of classical electrical or pharmacological interventions, as they allow cell-type-specific manipulations of biochemical or electrical processes with high spatiotemporal precision, which can be further refined by subcellular targeting strategies (Rost et al., 2017). We reasoned that targeting a photoactivated adenylyl cyclase to the presynaptic terminal would enable light-induced cAMP production in axonal terminals, triggering presynaptic plasticity. The small photoactivated adenylyl cyclase bPAC from *Beggiatoa* has several advantageous features for such an approach, as it is highly sensitive to blue light, shows low dark activity, exhibits a >100 fold increased activity in light, and is well expressed in neurons (Stierl et al., 2011). By fusing bPAC to the synaptic vesicle protein synaptophysin, we created synaptoPAC, a presynaptically targeted version of bPAC (Figure 1a). We demonstrate that light-triggered activation of synaptoPAC elicits presynaptic potentiation, both in autaptic cultures of hippocampal granule cells as well as in field-recordings of hippocampal MFs in acute brain slices. The effect of synaptoPAC activation was vastly different between synapses known for cAMP-dependent modulation of transmission and cAMP-insensitive synaptic terminals, highlighting the specificity of the optogenetic manipulation. Thus, synaptoPAC will likely be of great value for investigations on the mechanisms and functional implications of presynaptic plasticity.

FIGURE 1 Design and validation of synaptoPAC. (a) Illustration of the presynaptic targeting strategy for bPAC, and the optogenetic induction of presynaptic plasticity by synaptoPAC activation. hsyn: human synapsin promoter; FAD: flavin adenine dinucleotide. (b) Fluorescence images of an ND7/23 cell expressing synaptoPAC and SthK-EGFP. Scale bar: 10 μm. (c) 10 ms flashes of 474 nm light triggered intensity-dependent outward currents in ND7/23 cells co-expressing the cAMP-gated SthK channel together with synaptoPAC ($n = 8$, $N = 2$) or untargeted bPAC ($n = 8$, $N = 2$), but not in cells expressing synaptophysin-mKate2 and SthK. Scale bars: 200 pA, 20 s. (d) Immunofluorescence images of synaptoPAC-expressing cultured neurons stained for the dendritic marker MAP-2, mKate2 indicating synaptoPAC localization, and VGLUT1 as marker for glutamatergic presynaptic terminals. Scale bar: 20 μm. Close up of a dendrite reveals a signal overlap (white in merge) of mKate2 (magenta) and VGLUT1 (green). MAP2 is not shown in the merge. Scale bar: 2 μm. (e) Immunofluorescence images of cultured neurons expressing mKate2-bPAC. Scale bars: 20 μm and 2 μm for the close up. (f) The average synapse to dendrite ratio of the mKate2 signal was 4.7 times higher for synaptoPAC than for the untargeted mKate2-bPAC (synaptoPAC: 2.9 ± 1.2, $n = 15$; $N = 3$; mKate2-bPAC: 0.6 ± 0.5, $n = 12$; $N = 3$; $p < .0001$, Mann–Whitney U test).

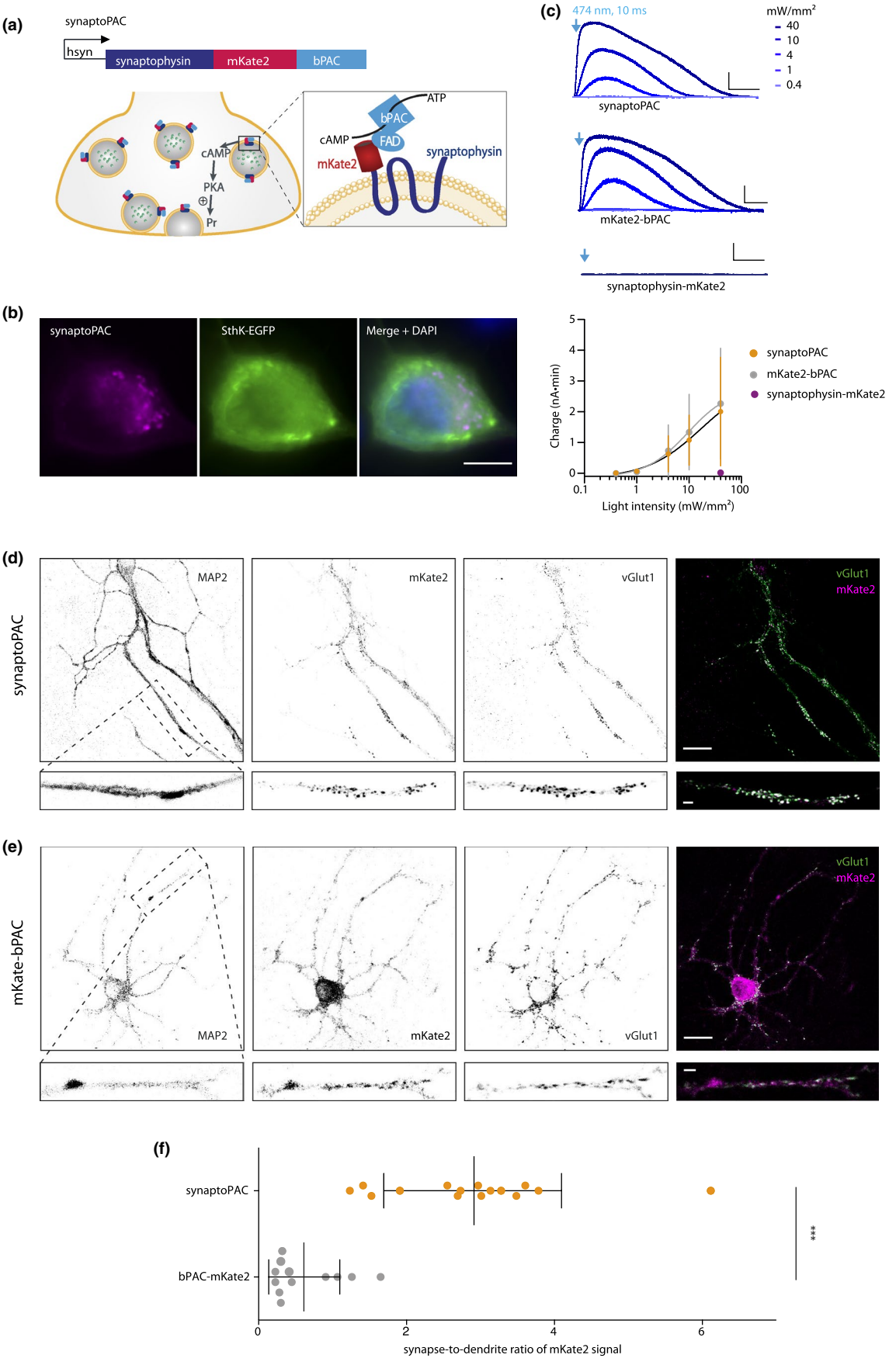
(a)
synaptoPAC
hsyn
synaptophysin
mKate2
bPAC
cAMP
PKA
Pr
ATP
bPAC
FAD
cAMP
mKate2
synaptophysin
(c)
474 nm, 10 ms
mW/mm²
40
10
4
1
0.4
synaptoPAC
mKate2-bPAC
synaptophysin-mKate2
(b)
synaptoPAC
SthK-EGFP
Merge + DAPI
Charge (nA·min)
Light intensity (mW/mm²)
synaptoPAC
mKate2-bPAC
synaptophysin-mKate2
(d)
synaptoPAC
MAP2
mKate2
vGlut1
vGlut1
mKate2
(e)
mKate-bPAC
MAP2
mKate2
vGlut1
vGlut1
mKate2
(f)
synaptoPAC
bPAC-mKate2
***
synapse-to-dendrite ratio of mKate2 signal

2 | MATERIALS AND METHODS

2.1 | Animal experiments

All animal experiments were carried out according to the guidelines stated in Directive 2010/63/EU of the European Parliament on the protection of animals used for scientific purposes and were approved by the local authorities in Berlin (Berlin state government/Landesamt für Gesundheit und Soziales, license number G0092/15, T0100/03 and T0073/04), Germany. Animals were bred in the Charité animal facility and housed in singularly ventilated cages of 4–10 mice on a 12-hr light-dark cycle with access to food and water *ad libitum*.

2.2 | Molecular biology

For initial tests in neuronal cell cultures, we fused the coding sequence of mKate2 and bPAC (from the soil bacterium *Beggiatoa*) to the 3' end of the rat synaptophysin coding sequence by Gibson assembly. The resulting fusion construct (synaptophysin-mKate2-bPAC) was then transferred into a lentiviral expression vector via

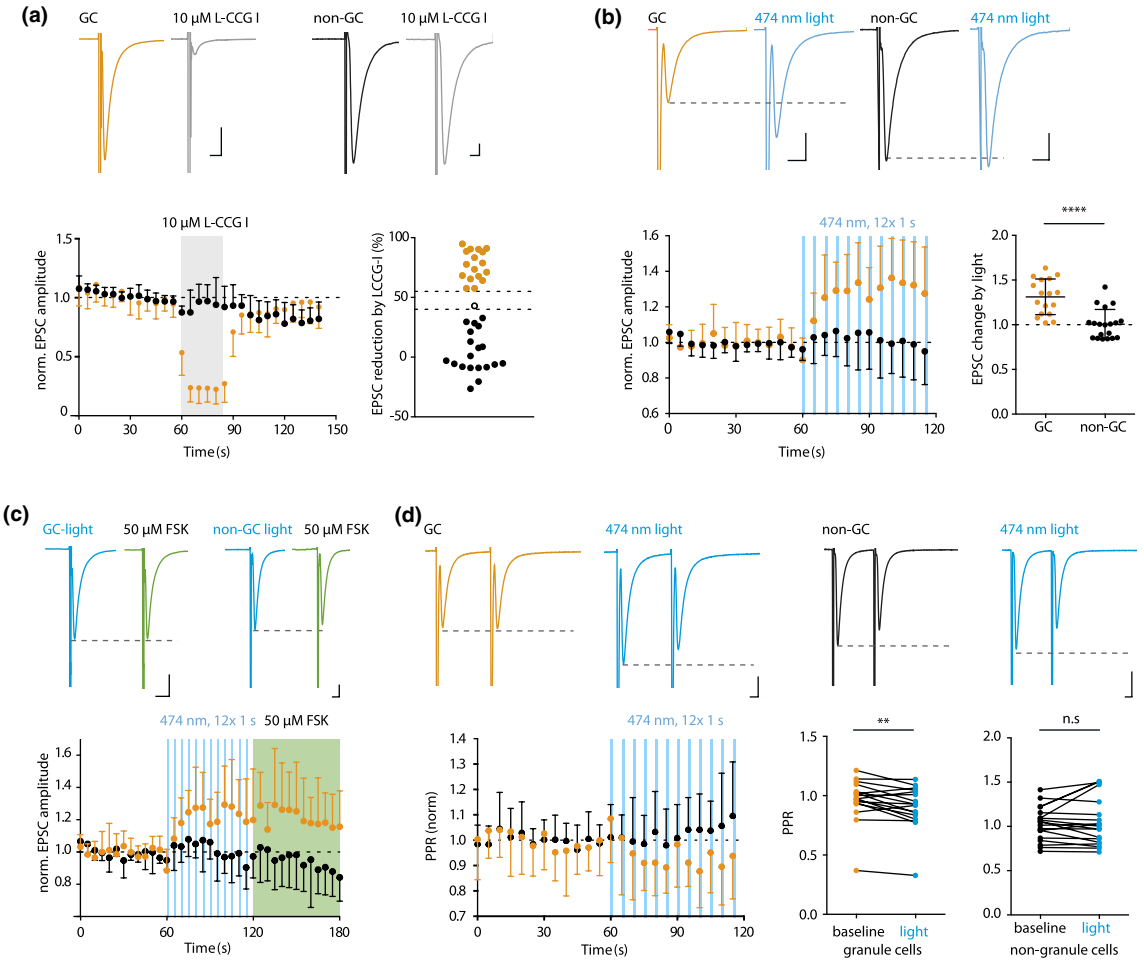

FIGURE 2 SynaptoPAC potentiates evoked synaptic transmission specifically in cultured hippocampal granule cells. (a) Example traces illustrating the effect of the group II metabotropic glutamate receptor agonist L-CCG I (10 µM) on two types of hippocampal excitatory neurons in autaptic cultures. Scale bars, 10 ms, 1 nA. Neurons in which L-CCG I decreased the EPSC amplitude by >55% were classified as granule cells (GCs). Cells with <40% reduction of the EPSC amplitude by L-CCG I were defined as non-granule cells (non-GCs), others (open circle) were not included in further analysis. Time plot shows the reversible L-CCG I effect on EPSC amplitudes recorded from GCs (orange; $n = 17$, $N = 4$) and non-GCs (black; $n = 19$, $N = 5$). (b) EPSCs recorded before and after synaptoPAC activation from a GC and non-GC. Scale bars: 10 ms, 1 nA. Light pulses (474 nm, 70 mW mm^{-2}, 12 × 1 s at 0.2 Hz) increased EPSC amplitudes in synaptoPAC-expressing GCs by 1.31 ± 0.19 (orange; $n = 17$, $N = 4$), but had no effect in synaptoPAC-expressing non-GCs (black; 1.00 ± 0.16, $n = 19$, $N = 5$; $p < .0001$; unpaired *t*-test). (c) Potentiation of EPSCs by activation of synaptoPAC (blue) and by subsequent application of 50 µM forskolin (FSK; green). Scale bars: 10 ms, 1 nA. In GCs, FSK increased the EPSC amplitude by 1.21 ± 0.07 (orange; $n = 10$, $N = 4$), not further increasing light induced potentiation. In non-GCs FSK did not increase EPSCs (0.94 ± 0.06; black; $n = 9$, $N = 3$). (d) Paired EPSCs evoked at 25 Hz in a GC (orange) and a non-GC (black). Scale bars: 1 nA, 10 ms. Light stimulation significantly decreased the paired-pulse ratio in GCs (baseline: 0.96 ± 0.18, light: 0.90 ± 0.18; $n = 17$, $N = 4$; $p = .005$; Wilcoxon test) but had no effect on the paired-pulse ratio in non-GC (baseline: 1.03 ± 0.18, light: 1.06 ± 0.27; $n = 19$, $N = 5$; $p = .5$, paired *t*-test).

PCR, which allowed expression under control of the neuron-specific human synapsin (hsyn) promoter. This construct was used for the characterization in neuronal cultures (Figures 1 and 2). Since mKate2-fluorescence was very weak and difficult to detect in live-cell imaging, we replaced the fluorophore with mCherry, and transferred the construct into an adeno-associated virus (AAV)-expression vector for more efficient expression of synaptoPAC *in vivo*. In a final step of optimization, we replaced mCherry with mScarlet, since mCherry caused unintended protein aggregations in neurons (data not shown). All viruses (lentivirus and AAV serotype 9) were provided by the Viral Core Facility at the Charité Berlin.

2.3 | Autaptic granule cell culture

Autaptic cultures of dentate gyrus granule cells were prepared as previously described (Rost et al., 2010). In brief, P0-P1 Wistar rats (RRID:RGD_8553003, in total 23 rats) of either sex were decapitated, and brains were removed and transferred into an ice-cooled petri dish. Dentate gyri were dissected by longitudinal separation from the rest of the hippocampus. Cells were isolated by Papain digestion followed by manual trituration, and subsequently plated on islands of glial cells at a density of 1.25×10^4 cells/cm^2 in 6-well plates in Neurobasal-A (cat. no. 10888022), supplemented with 2% B27 (cat. no. 17504001) and 0.2% penicillin/streptomycin (cat. no. 15140122; all Invitrogen/ Thermo Fisher Scientific, Waltham, MA). Lentiviral particles encoding synaptoPAC were added 1–4 days after plating. Cells were used for electrophysiological recordings after 15–21 days *in vitro*.

2.4 | Cell culture of ND7/23 cells

ND7/23 cells (ECACC 92090903, RRID:CVCL_425, Merck, Darmstadt, Germany, cat. no. 92090903) were newly purchased and used until passage 20. The cell line is not listed in the International Cell Line Authentication Committee (ICLAC) database of cross-contaminated or misidentified cell lines. We did not perform further authentication of the cell line in the laboratory. Cells were cultured in Dulbecco's Modified Eagle's Medium (DMEM, Thermo Fisher Scientific, cat. no. 21010046) supplemented with 10% fetal calf serum (Pan Biotech, cat. no. P40-37500) and 0.1% penicillin/streptomycin (Thermo Fisher Scientific, cat. no. 15140122) at 37°C, 5% CO_2. 24 hr prior to transfection, cells were seeded onto 15 mm coverslips coated with collagen and poly-D-lysine. Cells were transfected using X-tremeGENE 9 (Sigma-Aldrich/ Merck, cat. no. 6365787001) at a ratio of 3:1 µl/µg DNA according to the manufacturer's protocol. Plasmids encoding PAC constructs and SthK-EGFP were used at a 3:1 ratio, and premixed before addition of the transfection reagent. Two days after transfection we performed whole-cell voltage clamp recordings on transfected cells identified by red fluorescence.

2.5 | Immunocytochemistry

At DIV 15–21, cultured neurons were fixed with 4% PFA in PBS for 10 min, then washed 3 times in PBS. Samples were permeabilized with 0.5% Triton-X100 for 5 min and blocked for 30 min in 2% normal goat serum in 0.1% Triton-X100. Samples were incubated with rabbit anti-RFP (against mKate2; 1:200; Thermo Fisher Scientific, cat. no. MA5-15257), mouse anti-microtubule-associated protein 2, clone 5F9 (MAP2; 1:100 Millipore/ Merck, cat. no. 05-346), and guinea pig anti-vesicular glutamate transporter 1 (VGLUT1; 1:4,000; Synaptic Systems, Göttingen, Germany, cat. no. 135304) primary antibodies at room temperature for 1.5 hr. Coverslips were washed 3 times with PBS before incubation with secondary antibodies conjugated with AlexaFluor-488, −555, or −647 (1:500; Invitrogen/ Thermo Fisher Scientific, cat. no. A11073, A27039, A27040) at room temperature for 1 hr. Finally, coverslips were washed 3 times with PBS and mounted in Mowiol (Carl Roth, Karlsruhe, Germany, cat. no. 0713.1).

2.6 | Confocal microscopy

Neurons were imaged on an upright TCS SP5 confocal microscope (Leica Microsystems, Wetzlar, Germany). The following laser lines were used to illuminate fluorescent specimens through a 63x oil immersion objective (1.4 NA): 488 nm (Argon laser), 568 nm (solid state), and 633 nm (Helium, Neon). Images of 1,024 × 1,024 pixels were acquired with 5x zoom at 400 Hz, with a 16x line average for the mKate2 signal. We quantified presynaptic enrichment of bPAC-constructs by calculating the ratio of the mKate2 signal in VGLUT1-positive spots (presynaptic terminals) and the mKate2 signal in VGLUT1-negative, but MAP2-positive areas (dendrites). For each cell, we created 4x4 pixel regions of interest (ROIs) on 20 VGLUT1-positive spots, and 20 ROIs on MAP2-positive, but VGLUT1-negative spots, using the Time Series Analyzer plugin (https://imagej.nih.gov/ij/plugins/time-series.html) in Fiji. For these ROIs, we measured the mean grey value in a single-plane confocal image of the mKate2 channel. After background subtraction, we then calculated the synapse to dendrite ratio of the averaged mKate2 signal in VGLUT1-positive spots to the averaged mKate2 signal in MAP2-positive spots.

2.7 | Electrophysiology of ND7/23 cells and neuronal cultures

Whole-cell voltage clamp recordings were performed on an IX73 inverted microscope (Olympus, Shinjuku, Tokyo, Japan) using a Multiclamp 700B amplifier under the control of a Digidata 1550 AD board and Clampex 10 software (all Molecular Devices). All recordings were performed at room temperature. Data were acquired at 10 kHz and filtered at 3 kHz. A TTL-controlled LED system (pE4000, CoolLED, Andover, UK) was coupled into the back port of the IX73

microscope by a single liquid light guide. Fluorescent light was passed through a quad band filter set (AHF, Tübingen, Germany, cat. no. F66-415) and an Olympus UPLSAPO 20×, NA 0.75 objective. For visualization of mKate2 fluorescence, we used a triple band filter set (AHF, cat. no. F66-502) with 575/25 nm excitation filter. Extracellular solution contained (in mM): 140 NaCl, 2.4 KCl, 10 HEPES, 10 glucose, 2 $CaCl_2$, and 4 $MgCl_2$ (pH adjusted to 7.3 with NaOH, 300 mOsm). The intracellular solution contained (in mM): 135 K-gluconate, 17.8 HEPES, 1 EGTA, 4.6 $MgCl_2$, 4 Na_2ATP, 0.3 NaGTP, 12 disodium phosphocreatine, and 50 U/ml creatine phosphokinase, pH adjusted to 7.3 with KOH, 300 mOsm. Unless otherwise stated, all chemicals were purchased from Tocris, Merck or Carl Roth.

ND7/23 cells co-expressing SthK-EGFP and synaptoPAC, mKate2-bPAC, or synaptophysin-mKate2 were voltage clamped at −60 mV. Photoactivated adenylyl cyclases were stimulated by 10 ms flashes of 474 nm light with varying intensity, which elicited cAMP-triggered K^+ currents.

In whole-cell voltage clamp recordings from cultured neurons, membrane potential was set to −70 mV. Paired EPSCs were evoked every 5 s by triggering two unclamped action potentials at 25 Hz using 1 ms depolarizations of the soma to 0 mV. Granule cells were distinguished from other glutamatergic hippocampal neurons by their sensitivity of synaptic transmission to application of the group II metabotropic glutamate receptor agonist L-CCG I ((2S,1'S,2'S)-2-(Carboxycyclopropyl)glycines; 10 μM; Tocris, Bristol, UK, cat. no. 0333). We classified neurons as granule cells if L-CCG I reduced their transmission by >55%, and neurons which showed <40% reduction of the EPSC as non-granule cells, while neurons with an intermediate effect on transmission were not included in further analysis (Figure 2a). The reduction of EPSC amplitudes by L-CCG I was calculated from the last four sweeps under L-CCG I and the last four sweeps from baseline before drug application. SynaptoPAC was activated by 12 flashes (1 s) of 474-nm light at 0.2 Hz at 70 mW mm^{-2}. The paired-pulse ratio was calculated as the ratio from the second and first EPSC amplitude with an interstimulus interval of 40 ms. Data were analyzed using AxoGraph X (AxoGraph, Sydney, Australia). EPSC potentiation and paired-pulse ratio changes by light stimulation or forskolin treatment were calculated from the average of 12 EPSCs during baseline and the last 6 EPSCs during the stimulation. For detection of miniature EPSCs, we filtered the recordings post hoc with a digital 1-kHz low-pass filter, and applied a template-based algorithm implemented in AxoGraph X. Frequency and amplitude of mEPSCs were corrected for false positives events, which we estimated by running the event detection with an inverted template (Rost et al., 2015). Recordings were excluded from the mEPSC analysis if false-positive events occurred at a frequency of >1 Hz.

2.8 | Stereotactic surgeries

Wild-type C57BL/6N mice (P25–P31; Charles River Strain Code 027) of both sexes were injected with 200 nl of AAV9.hsyn:synaptophysin-mScarlet-bPAC using a NanoFil syringe with a 34-gauge needle (with UMP3 microinjection system and Micro4 controller; all from World Precision Instruments) at a rate of 40 nl/min. After the injection, the needle remained in position for another 5 min before it was slowly withdrawn. Mice were anesthetized under isoflurane (1.5% vol/vol in oxygen) during surgery and body temperature was maintained at 37°C. Animals received a subcutaneous injection of Carprofen (5 mg/kg) during the surgeries for analgesia. Injections were aimed at the following coordinates relative to bregma: anteroposterior (AP): 1.93 mm, mediolateral (ML): ±1.5 mm, dorsoventral (DV): −2.0 mm for the DG; AP: 1.75 mm, ML: 2.00 mm, DV: −2.1 mm for CA3. All animals were allowed to recover for at least 3 weeks before slice preparations and recording.

2.9 | Electrophysiology on hippocampal slices

Animals were anesthetized under isoflurane and decapitated. Under continuous safe light illumination, brains were quickly removed and placed in ice-cold sucrose-based artificial cerebrospinal fluid (sACSF) containing (in mM): 50 NaCl, 25 $NaHCO_3$, 10 glucose, 2.5 KCl, 7 $MgCl_2$, 1 NaH_2PO_4, 0.5 $CaCl_2$, and 150 sucrose, saturated with 95% O_2 and 5% CO_2. Tissue blocks containing the hippocampal formation were mounted on a vibratome (Leica VT 1200S, Leica Microsystems). Sagittal slices were cut at 300-μm thickness and incubated in sucrose-based ACSF at 35°C for 30 min. Before the recording, slices were transferred into a submerged chamber filled with ACSF containing the following (in mM): 119 NaCl, 26 $NaHCO_3$, 10 glucose, 2.5 KCl, 1.3 $MgCl_2$, 1 NaH_2PO_4, and 2.5 $CaCl_2$, saturated with 95% O_2 and 5% CO_2. Slices were stored in ACSF for 0.5–6 hr at room temperature. A total of 34 mice were used for the slice experiments.

MF fEPSP recordings were performed at 21–24°C in a submerged recording chamber perfused with ACSF. Unless noted otherwise, MFs were stimulated at 0.05 Hz using a low-resistance glass electrode filled with ACSF, which was placed close to the internal side of granule cell layer of the dentate gyrus. The recording electrode filled with ACSF was placed in *stratum lucidum* of area CA3. The MF origin of fEPSPs was verified by the pronounced facilitation of synaptic response amplitudes upon 1 Hz stimulation or paired pulse stimulation at 25 Hz. In addition, we confirmed that fEPSPs were generated specifically by MFs by application of the type II metabotropic glutamate receptor agonist DCG IV ((2S,2'R,3'R)-2-(2',3'-dicarboxycyclopropyl) glycine; 1 μM, Tocris, Bristol, UK, cat. no. 0975) at the end of each recording. DCG IV specifically suppresses transmitter release from MF terminals in CA3, but not from neighboring associational-commissural fiber synapses (Kamiya et al., 1996). Only responses that were inhibited by >80% were accepted as MF signals (16 slice excluded).

Recordings from Schaffer collateral synapses in CA1 were performed at 21–24°C in a submerged recording chamber perfused with ACSF at 2 ml/min. The stimulation electrode was placed in *stratum radiatum* proximal to the CA3 area and the recording electrode in the

stratum radiatum of CA1. Field EPSPs were stimulated at 0.05 Hz. A stable baseline of fEPSP amplitudes was recorded for at least 10 min before optical stimulation. In CA1 fEPSP recordings, we verified the fidelity of synaptic plasticity at the end of each recording (>30 min post optical stimulation) by electrically inducing LTP by four high frequency trains (100 pulses at 100 Hz, 10 s inter train interval). Only experiments in which we recorded >10% increase of the fEPSP 20–30 min after tetanic stimulation were included in the analysis (3 recordings excluded). As a measure for unstable stimulation conditions, we analyzed the magnitude of the presynaptic fiber volley and rejected recordings in which the fiber volley changed >10% over the course of the whole recording (1 recording excluded).

In both types of recordings, optical potentiation was induced by 10 pulses of blue light at 0.05 Hz from a 470 nm LED (pE300, CoolLED), which was passed through a 474/23 nm filter (AHF, cat. no. F39-474). Light was applied via an Olympus LUMPLFLN 40x (NA 0.8) water immersion objective, which was placed in *stratum lucidum* of CA3 for MF recordings and in *stratum radiatum* of CA1 for Schaffer collateral recordings. Data was acquired using a Multiclamp 700B amplifier, Digidata 1550A AD board, and Clampex 10.0 recording software (all Molecular Devices). In some recordings, data were acquired using a Multiclamp 700B amplifier, a BNC-2090 interface board with PCI 6035E A/D board (National Instruments) and IGOR Pro 6.12 as recording software (WaveMetrics, Lake Oswego, OR). Signals were sampled at 10 kHz and filtered at 3 kHz. Recordings were analyzed using Clampfit (Molecular Devices), IGOR Pro, or Axograph X.

2.10 | Statistics

No randomization or blinding was performed in the study. We did not perform a power analysis to determine sample size prior to the experiments, since the aim of our study was to establish a new technology without prior knowledge on effect size and variability. Statistical analyses were performed with GraphPad Prism 5.0 and 6.0 (Graphpad Software). Normality of data was assessed using D´Agostino-Pearson test and no test for outliners was conducted. Data are presented as mean ± *SD*. N states the number of independent cell culture preparations or number of animals; and n states the number of cells recorded in cultures, or number of slices in fEPSP recordings.

3 | RESULTS

3.1 | SynaptoPAC design and functional validation

For the presynaptic targeting of bPAC we adopted a strategy previously established for optogenetic tools and fluorescent sensors (Granseth et al., 2006; Rost et al., 2015): By fusing bPAC together with a red fluorophore to the cytosolic C-terminus of the synaptic vesicle protein synaptophysin, we created synaptoPAC, a presynaptically targeted version of bPAC (Figure 1a). When coexpressed with the cAMP-sensitive K^+-channel SthK (Brams et al., 2014) in ND7/23 cells, light-activation of synaptoPAC triggered outward currents similar to untargeted bPAC, demonstrating efficient cAMP production by the enzyme (Figure 1b and c). No photocurrents were detected in cells co-expressing SthK and synaptophysin fused to mKate2 (Figure 1c). In cultures of rat hippocampal neurons, costainings for the glutamatergic vesicle marker VGLUT1 revealed a punctate expression of synaptoPAC, largely overlapping with VGLUT1 (Figure 1d), in contrast to a more diffuse expression pattern of the non-targeted bPAC-mKate2 (Figure 1e). We determined the synapse to dendrite ratio of the mKate2 signal from each cell as a measure of the relative presynaptic accumulation of the constructs (see Methods for details). The synapse to dendrite ratio was 2.9 ± 1.2 for synaptoPAC, but only 0.6 ± 0.5 for mKate2-bPAC, indicating a 4.8-fold enrichment of synaptoPAC at presynaptic terminals compared to untargeted bPAC (Figure 1f). Taken together, the fusion of bPAC to synaptophysin does not interfere with its enzymatic function and facilitates presynaptic accumulation of the construct.

Next, we wanted to test whether the presynaptically targeted, photoactivated adenylyl cyclase could enable light-triggered potentiation of transmitter release. In autaptic cultures of hippocampal granule cells stimulation of endogenous adenylyl cyclases by forskolin induces potentiation of transmitter release (Rost et al., 2010; Tong et al., 1996). We therefore chose this culture system as a test platform for establishing optogenetic potentiation of release by photocontrolled increase of presynaptic cAMP. We expressed synaptoPAC or synaptophysin-mKate2 as control in cultured hippocampal granule cells using lentivirus and performed whole-cell patch-clamp recordings 2–3 weeks post transduction. Hippocampal granule cells were identified by the specific suppression of their transmitter release by agonists of group II metabotropic glutamate receptors (Figure 2a, see Methods for details). Importantly, overexpression of neither synaptophysin-mKate2 nor synaptoPAC had any effect on excitatory postsynaptic currents (EPSCs), readily releasable pool, release probability, or short-term plasticity of transmitter release (Figure S1). After pharmacological characterization of the neuronal cell-type and recording a stable baseline of evoked transmission, we triggered synaptoPAC-mediated cAMP production with 12 1-s pulses of blue light at 0.2 Hz. Photostimulation increased EPSC amplitudes to 131 ± 19% of baseline in granule cells, but had no effect on transmission in non-granule cells (Figure 2b), indicating that the potentiation of synaptic transmission via photo-induced production of cAMP might be a cell-type-specific effect. We found no light-triggered potentiation in synaptophysin-expressing granule cells, which however, showed robust potentiation by forskolin (Figure S2a–c). In contrast, glutamatergic transmission of pyramidal neurons did not increase under forskolin (Figure 2c). In synaptoPAC-expressing granule cells, blue-light illumination occluded a further increase of EPSCs by forskolin (Figure 2c). Conversely, light-stimulation did not further increase EPSC amplitudes after forskolin treatment (Figure S2d–f). These findings indicate that both the pharmacologically as well as the

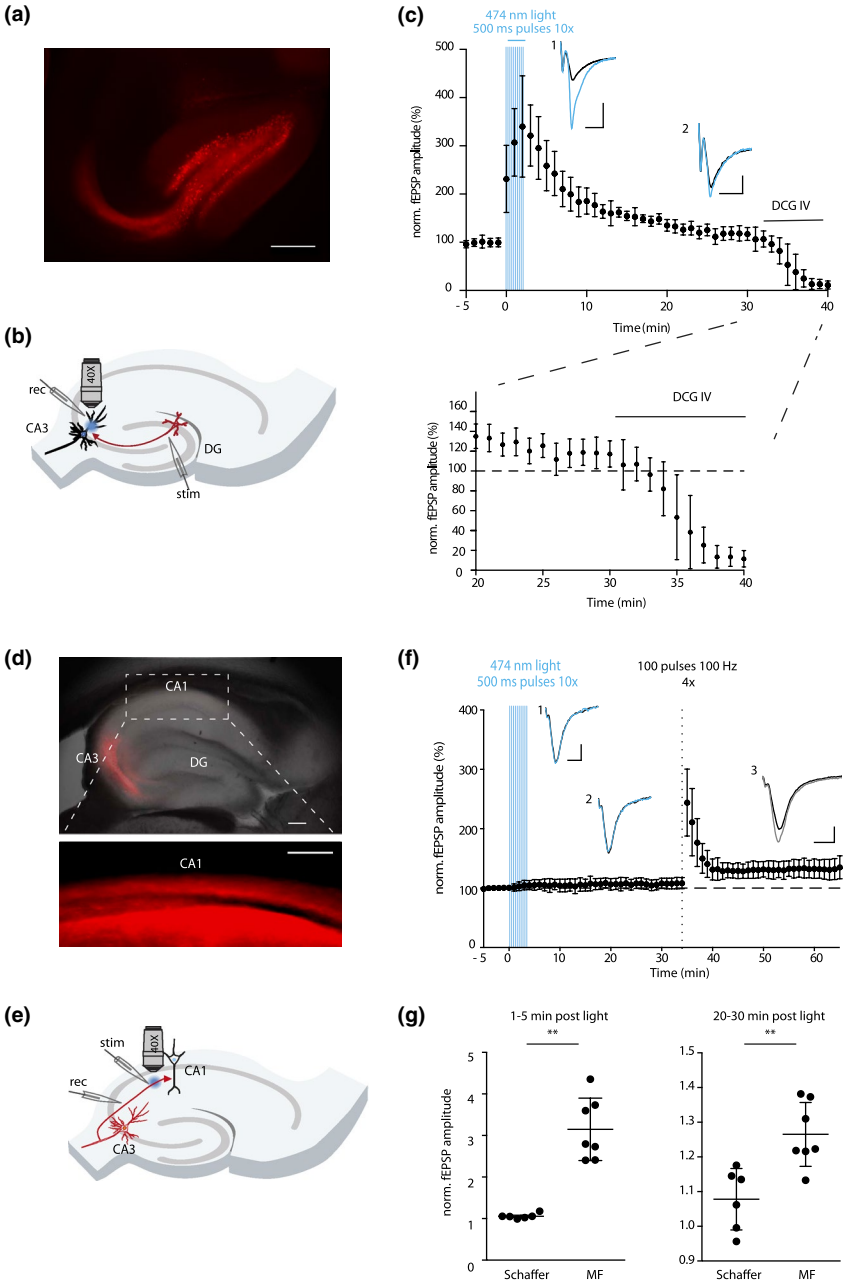

FIGURE 3 SynaptoPAC activation increases transmission at MF-CA3, but not at Schaffer collateral-CA1 synapses. (a) Fluorescent image of mScarlet confirming synaptoPAC expression in the dentate gyrus and MFs. Scale bar, 200 μm. (b) Schematic illustration of the recording configuration in acute hippocampal slices for MF-CA3 synapses, with optical stimulation in *stratum lucidum* in CA3. (c) Optical activation with 500 ms pulses of 474 nm light (11 mW mm^{-2}, repeated 10 times at 0.05 Hz) acutely increased MF fEPSPs to 313 ± 75% of baseline, and triggered potentiation of MF fEPSPs (126 ± 9%) lasting >20 min. Example traces showing baseline synaptic transmission (black), (1) potentiated transmission in the first 5 min after illumination (blue; scale bar: 200 μV, 20 ms), and (2) LTP after 20–30 min (scale bar: 100 μV, 20 ms). Only experiments that showed >80% reduction of fEPSP amplitudes by application of DCG IV (1 μM) were considered as MF recordings ($n = 7$ slices, 6 mice). (d) Overlay of DIC and fluorescent image showing synaptoPAC expression in area CA3 and in Schaffer collaterals (inset). Scale bars: 200 μm. (e) Scheme of the recording configuration at Schaffer collateral-CA1 synapses. (f) In Schaffer collateral synapses expressing synaptoPAC, blue light stimulation had no immediate effect in the first 5 min post illumination (1) (104 ± 6% of baseline), nor did it cause strong LTP after 20–30 min (2) (107 ± 8%). However, these synapses showed post-tetanic potentiation of 192 ± 42% and long-term potentiation (3) (132 ± 15%) following 4 trains of 100 electrical stimuli at 100 Hz ($n = 6$ slices, 3 mice). Scale bars: 100 μV, 10 ms. (g) Direct comparison of the synaptoPAC effect on transmission at MF-CA3 and CA3-CA1 synapses. In both cases the effect size induced by synaptoPAC is significantly higher in MF synapses compared to Schaffer collaterals synapses (1–5 min: $p = .0006$; 20–30 min: $p = .02$, both Mann–Whitney test). Data points shown in (c) and (f) are binned to 1 min.

optogenetically driven increase of cAMP saturate the downstream signaling cascade for presynaptic potentiation in granule cells. The optogenetic potentiation also altered the short-term plasticity of synaptic transmission, by reducing the amplitude ratio of two EPSCs evoked at 25 Hz (Figure 2d). This decrease in paired-pulse ratio (PPR) indicates a presynaptic origin of the effect, and often correlates with an increase in the release probability (Abbott & Regehr, 2004; Zucker & Regehr, 2002). In contrast, synaptoPAC activation did not alter the PPR in non-granule cells. Of note, light-triggered elevation of presynaptic cAMP increased the frequency of miniature EPSCs (mEPSCs), but did not affect mEPSC amplitudes, independent of the cell type (Figure S3). In summary, our experiments in neuronal cultures indicate that synaptoPAC acts via a presynaptic mechanism and increases evoked release in a cell-type-specific manner.

3.2 | SynaptoPAC potentiates transmission at MF-CA3 synapses

Next, we tested whether synaptoPAC was able to potentiate transmission at hippocampal MF-CA3 synapses, the classical preparation to study presynaptic forms of LTP. We injected AAVs encoding synaptoPAC into the dentate gyrus of wildtype mice *in vivo*. After three to four weeks, we prepared acute hippocampal slices, and found strong synaptoPAC expression in dentate gyrus granule cells and the MF tract (Figure 3a). We electrically stimulated MF transmission and recorded field excitatory postsynaptic potentials (fEPSPs) in area CA3. SynaptoPAC was activated by applying blue light pulses locally at MF terminals through a 40x objective in the area of the recording electrode (Figure 3b). During an initial screening (Figure S3a and b) we tested several activation protocols for synaptoPAC and found robust potentiation with 10 pulses of 474 nm light, 11 mW mm^{-2}, applied at 0.05 Hz, with 0.5 s pulse duration (total light dosage: 55 mW mm^{-2}). MF fEPSP amplitudes increased to 313 ± 75% within 5 min after the start of the optical induction protocol (Figure 3c). Subsequently, fEPSPs decreased but were still potentiated by 126 ± 9% after 20–30 min post induction. In a separate set of experiments we found that a 10x lower light dosage (5.5 mW s mm^{-2}) was equally effective for stimulating synaptic potentiation (Figure S4; post-light potentiation: 363 ± 57%, potentiation after 20–30 min: 130 ± 6.5%), indicating that a wide range of light intensities is suitable for the activation of synaptoPAC. At the end of each recording we verified the MF origin of the signal by applying the metabotropic glutamate receptor agonist DCG-IV (Figure 3c), which specifically suppresses release from MF terminals, but not from neighboring associational-commissural fiber synapses in CA3 (Kamiya et al., 1996). Next, we examined whether synaptoPAC-induced plasticity was specific for synapses that express cAMP-dependent presynaptic LTP. For this we expressed synaptoPAC in CA3 pyramidal neurons (Figure 3d and e), and recorded fEPSPs from Schaffer collateral synapses in CA1, which express an NMDA (N-methyl-D-aspartate) receptor-dependent, postsynaptic form of LTP (Herring & Nicoll, 2016). Activation of synaptoPAC with the same light pulse protocol (total light dosage: 55 mW s mm^{-2}) that elicited strong potentiation in MF-CA3 synapses did not induce significant potentiation on Schaffer collateral synapses (Figure 3f and g), however, these synapses showed potentiation following tetanic electrical stimulation (Figure 3f). Together, the experiments in acute hippocampal slices confirm a synapse-specific effect of synaptoPAC.

3.3 | SynaptoPAC activation alters presynaptic release probability

One of the distinguishing characteristics of MF-CA3 synapses is the pronounced short-term facilitation of synaptic transmission upon repetitive activation (Nicoll & Schmitz, 2005). Presynaptic LTP at MF-CA3 synapses reduces the dynamic range of the short-term plasticity of release (Gundlfinger et al., 2007; Weisskopf et al., 1994; Zalutsky & Nicoll, 1990). To test whether optogenetic potentiation similarly alters MF release properties, we tested short-term plasticity of MF fEPSPs using two different protocols: 5 pulses at 25 Hz and 20 pulses at 1 Hz, both before and after blue-light stimulation (Figure 4a). Indeed, illumination significantly decreased both the PPR of the second to the first and of the fifth to the first fEPSP in the 25 Hz burst (Figure 4b). Optogenetic potentiation also caused a significant decrease of the frequency facilitation that is observed when increasing stimulation frequency from 0.05 Hz to 1 Hz (Figure 4c). Both test protocols indicate that synaptoPAC-driven MF potentiation changes the release probability. Control recordings of MF fEPSPs in hippocampal slices from non-injected wildtype mice demonstrated that the dynamics of short-term plasticity of MF transmission were not decreasing when tested repetitively (Figure S5a and b). Of note, the 1 Hz frequency facilitation in slices from non-infected control animals was similar to that observed in slices from synaptoPAC-expressing animals (control: 4.3 ± 1.2, synaptoPAC: 4.4 ± 2.3), indicating that overexpression of synaptoPAC itself did not alter MF release properties. In a subset of recordings, we also applied forskolin, which triggered a 2.4 ± 1 fold increase in fEPSP amplitude, and in turn significantly reduced both frequency facilitation and paired-pulse facilitation (Figure S5c–e), confirming previous reports (Huang et al., 1994; Weisskopf et al., 1994). Taken together, synaptoPAC enables light-controlled production of cAMP at presynaptic terminals, which leads to an increase in transmitter release specifically at synapses sensitive to cAMP.

4 | DISCUSSION

Tools enabling selective and remote-controlled induction of presynaptic plasticity are required to elucidate the mechanisms and functional relevance of presynaptic LTP (Monday et al., 2018). SynaptoPAC, a fusion of the photoactivated adenylyl cyclase bPAC to the synaptic vesicle protein synaptophysin, is well suited for such investigations: We demonstrate that overexpression of synaptoPAC does not affect synaptic transmission, and that the optogenetic

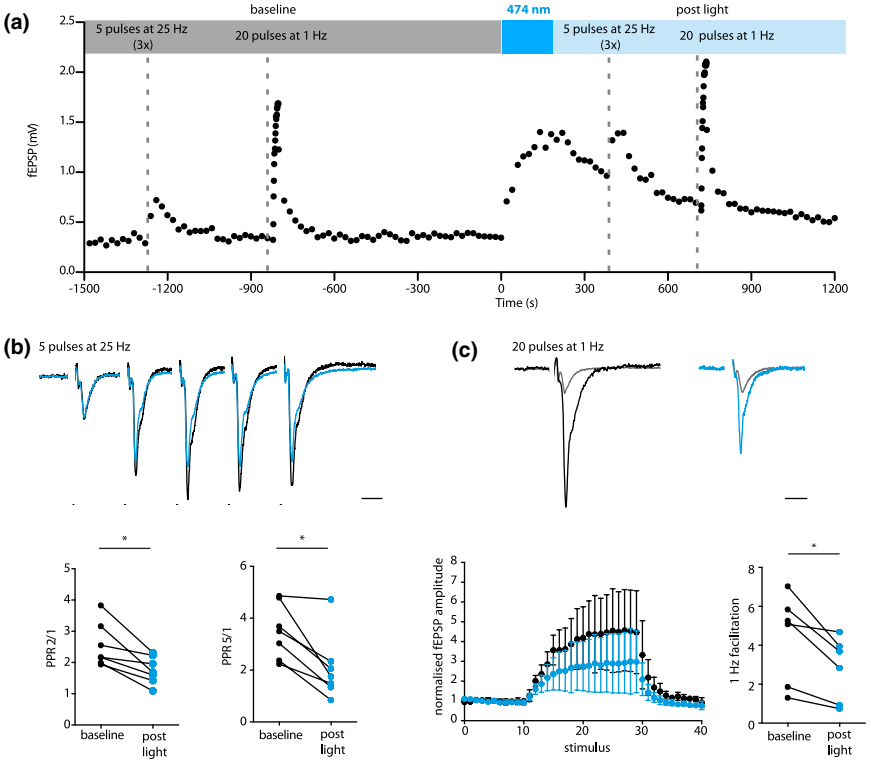

FIGURE 4 SynaptoPAC mediates potentiation by a presynaptic mechanism. (a) Typical representation of the recording protocol for MF short-term plasticity: MF were first stimulated electrically with 5 pulses at 25 Hz and with 20 pulses at 1 Hz. Following synaptoPAC activation by 10 pulses of 474 nm light (500 ms, 11 mW mm^{-2}, 0.2 Hz), the 25 Hz and 1 Hz stimulus trains were applied again 5 and 10 min after optical induction, respectively. For the 25 Hz trains, only the first fEPSP amplitude was plotted. (b) Representative traces of five MF fEPSP elicited at 25 Hz before (black) and after light stimulation (blue), scaled to the amplitude of the first fEPSP. Scale bar: 20 ms. SynaptoPAC induced potentiation significantly decreased the paired-pulse ratio between the second and the first fEPSPs (baseline: 2.54 ± 0.7, post light: 1.76 ± 0.43; $n = 7$ slices, 6 mice; $p = .02$, Wilcoxon signed-rank test), and the fifth and first fEPSPs (baseline: 3.50 ± 1.05, post light: 2.08 ± 1.26; $p = .02$, Wilcoxon signed-rank test). (c) Traces showing the first and last MF fEPSP evoked by a train of 20 stimuli applied at 1 Hz before (black) and after (blue) blue-light illumination. Traces are normalized to the first fEPSP in the train. Scale bar: 20 ms. 1 Hz facilitation was significantly decreased after optogenetic potentiation (baseline: 4.40 ± 2.29, post light: 2.80 ± 1.64; $n = 7$ slices, 6 mice; $p = .03$, Wilcoxon signed-rank test).

production of cAMP is equally effective as pharmacological activation of endogenous adenylyl cyclases. Because of its small size, the construct is easily expressed *in vivo* via AAVs, which will allow for cell-type-specific expression through the use of Cre-lox recombination or cell-type-specific promoters. The highly light sensitive bPAC used in the synaptoPAC construct is selectively activated by blue light (Stierl et al., 2011), which enables experimental combinations with other optogenetic actuators and fluorescent sensors sensitive to light >520 nm (Bernal Sierra et al., 2018). A previous study in hippocampal pyramids revealed a stronger increase in cAMP levels by bPAC activation than by forskolin application, probably because of the limited capacity of the endogenous adenylyl cyclases activated by forskolin, which are bypassed by the photoactivated adenylyl cyclases (Stierl et al., 2011). However, this study analyzed cAMP-gated currents from overexpressed cyclic-nucleotide-gated channels, which are likely not saturated by endogenously produced cAMP. In our recordings from autaptic granule cells we found mutual occlusion of both forskolin- and synaptoPAC-induced potentiation of transmission, indicating that both manipulations saturate the signaling cascade downstream of cAMP (Figure 2c, Figure S2). In extracellular field recordings from MFs the post-light potentiation following synaptoPAC activation was higher than forskolin-induced potentiation, but not statistically different (synaptoPAC (Figure 3c): 313 ± 75%; forskolin (Figure S5e): 240 ± 97%; $p = .13$, Mann–Whitney U test). Importantly, we show that local illumination of axonal terminals is sufficient to trigger potentiation, allowing target area-specific manipulations. In summary, our results suggest that synaptoPAC is at least as effective as the classical pharmacological induction of presynaptic LTP by forskolin, with the advantage that the manipulation by optogenetic stimulation is clearly confined to the presynaptic compartment.

Interestingly, the time course of synaptoPAC-mediated potentiation of MF transmission in hippocampal slices (Figure 3c, Figure S4c) matches the time course of post-tetanic potentiation induced by electrical stimulation with regular high frequency trains or naturally occurring activity patterns (Gundlfinger et al., 2010; Vandael et al., 2020), with a strong initial increase that decays with a tau of approx. 20 min. Our data demonstrate

that at MF terminals a transient increase of presynaptic cAMP in the absence of high-frequency action potential firing is sufficient for synaptic potentiation, in contrast to CA3-CA1 synapses, where a selective increase of presynaptic cAMP by synaptoPAC is not sufficient to potentiate action potential-evoked transmission (Figure 3). Previously, forskolin in combination with phosphodiesterase inhibitors was used to increase transmission at CA3-CA1 synapses (Chavez-Noriega & Stevens, 1992, 1994; Frerking et al., 2001; Otmakhov et al., 2004). However, it is unclear whether this form of chemical potentiation is purely presynaptic, if physiological activity can recapitulate the pharmacological stimulation, and to which extend cAMP-independent effects of forskolin contribute to it (Laurenza et al., 1989). In our hands, a selective increase of presynaptic cAMP by optogenetic means without pharmacological inhibition of phosphodiesterases did not induce strong potentiation at Schaffer collateral synapses nor in cultures of hippocampal non-granule cells. Our findings suggest that Schaffer collateral synapses not just lack presynaptic adenylyl cyclases but differ in key features of the molecular machinery required for presynaptic long-term plasticity, resulting in a synapse-specific effect of cAMP on evoked transmission. Of note, and in line with previous reports (Maximov et al., 2007; Steuer Costa et al., 2017), synaptoPAC-driven elevation of presynaptic cAMP increased mEPSC frequency, irrespective of the glutamatergic cell type. Presynaptic cAMP promotes synapsin phosphorylation by PKA, causing dissociation of synapsin from vesicles, and spatial reorganization of vesicles in the terminal (Menegon et al., 2006; Patzke et al., 2019; Vaden et al., 2019). In future, optogenetic control of presynaptic cAMP by synaptoPAC will provide novel avenues to study such kinds of vesicle pool regulation.

SynaptoPAC-driven enhancement of release will be useful to study computational aspects of presynaptic potentiation, which alters short-term synaptic filtering dynamics by shifting spike transmission from a high-pass toward a low-pass mode (Abbott & Regehr, 2004). How this altered synaptic computation affects encoding, storage and recall of associative memories is mostly unknown (Rebola et al., 2017). So far, causative behavioral studies have relied on either genetic ablation of major presynaptic molecules, or drugs of abuse acting on presynaptic metabotropic receptors such as cannabinoids, opioids, and cocaine (for review see Kauer & Malenka, 2007; Monday et al., 2018). However, genetic deletions act on very long time scales, and both genetic and pharmacological manipulations may have systemic effects. It is therefore difficult to unambiguously relate these interventions to synaptic alterations and behavioral consequences. Presynaptic plasticity has also been associated with pathophysiological brain conditions such as schizophrenia, autism spectrum disorders, and addiction, but it remains unclear whether aberrant presynaptic plasticity contributes causally or results from the disease (Monday & Castillo, 2017). We expect that synaptoPAC represents a versatile optogenetic tool to unravel some of the outstanding questions of presynaptic plasticity, both under physiological and pathophysiological conditions.

5 | COMPETING INTERESTS

The authors declare no competing interests. AAV expression vectors for synaptoPAC are available on Addgene.org (plasmid #153100 and #153085).

ACKNOWLEDGMENTS

The authors thank Katja Pötschke, Bettina Brokowski, Anke Schönherr, Susanne Rieckmann and Katja Czieselsky for excellent technical assistance, and Felicitas Brüntgens for help with the neuronal cell culture. The authors thank Rosanna Sammons for comments on the manuscript. This work was supported by grants from the Deutsche Forschungsgemeinschaft (DFG; German Research Foundation) under Germany's Excellence Strategy – EXC-2049 – 390688087 to D.S. and C.R., SPP 1926 (B.R.R), SPP 1665 (D.S.), SFB 1315 (D.S.), SFB 958 (C.R., D.S.). The plasmid encoding bPAC was kindly provided by the laboratory of Peter Hegemann, Humboldt University Berlin, Germany. SthK-EGFP was kindly provided by Franziska Schneider-Warme, Institute for Experimental Cardiovascular Medicine, University of Freiburg, Germany. A previous version of this manuscript was posted on bioRxiv (www.biorxiv.org/content/10.1101/2020.03.27.011635v1).

Open access funding enabled and organized by ProjektDEAL.

All experiments were conducted in compliance with the ARRIVE guidelines.

AUTHORS' CONTRIBUTIONS

S.O., L.M-V., L.F., A.S., and B.R.R performed the experiments. S.O., L.F., and B.R.R. analyzed the data. B.R.R. designed the tool, and B.R.R., D.S., and C.R. conceptualized the research. B.R.R and D.S. acquired funding for the project and supervised the work. B.R.R and S.O. wrote the paper with input from all authors. All authors approved submission of the manuscript.

OPEN RESEARCH BADGES

This article has received a badge for *Open Materials* because it provided all relevant information to reproduce the study in the manuscript. More information about the Open Science badges can be found at pAAv—syn-synaptoPAC-minWPRE: https://www.addgene.org/153085/ and pAAV-syn-FLEX-synaptoPAC-minWPRE: https://www.addgene.org/153100/

ORCID

Silvia Oldani https://orcid.org/0000-0002-9034-6237
Laura Moreno-Velasquez https://orcid.org/0000-0001-9735-0039
Lukas Faiss https://orcid.org/0000-0001-5150-5541
Alexander Stumpf https://orcid.org/0000-0002-1510-6970
Christian Rosenmund https://orcid.org/0000-0002-3905-2444
Dietmar Schmitz https://orcid.org/0000-0003-2741-5241
Benjamin R. Rost https://orcid.org/0000-0003-1906-0081

REFERENCES

Abbott, L. F., & Regehr, W. G. (2004). Synaptic computation. *Nature*, *431*, 796–803. https://doi.org/10.1038/nature03010

Bernal Sierra, Y. A., Rost, B. R., Pofahl, M., Fernandes, A. M., Kopton, R. A., Moser, S., Holtkamp, D., Masala, N., Beed, P., Tukker, J. J., Oldani, S., Bönigk, W., Kohl, P., Baier, H., Schneider-Warme, F., Hegemann, P., Beck, H., Seifert, R., & Schmitz, D. (2018). Potassium channel-based optogenetic silencing. *Nature Communications*, *9*, 4611. https://doi.org/10.1038/s41467-018-07038-8

Brams, M., Kusch, J., Spurny, R., Benndorf, K., & Ulens, C. (2014). Family of prokaryote cyclic nucleotide-modulated ion channels. *Proceedings of the National Academy of Sciences*, *111*, 7855–7860. https://doi.org/10.1073/pnas.1401917111

Castillo, P. E. (2012). Presynaptic LTP and LTD of excitatory and inhibitory synapses. *Cold Spring Harbor Perspectives in Biology*, *4*, a005728–a005728. https://doi.org/10.1101/cshperspect.a005728

Castillo, P. E., Janz, R., Sudhof, T. C., Tzounopoulos, T., Malenka, R. C., & Nicoll, R. A. (1997). Rab3A is essential for mossy fibre long-term potentiation in the hippocampus. *Nature*, *388*, 590–593. https://doi.org/10.1038/41574

Castillo, P. E., Schoch, S., Schmitz, F., Sudhof, T. C., & Malenka, R. C. (2002). RIM1alpha is required for presynaptic long-term potentiation. *Nature*, *415*, 327–330.

Castro-Alamancos, M. A., & Calcagnotto, M. E. (1999). Presynaptic long-term potentiation in corticothalamic synapses. *Journal of Neuroscience*, *19*, 9090–9097. https://doi.org/10.1523/JNEUROSCI.19-20-09090.1999

Chavez-Noriega, L. E., & Stevens, C. F. (1992). Modulation of synaptic efficacy in field CA1 of the rat hippocampus by forskolin. *Brain Research*, *574*, 85–92. https://doi.org/10.1016/0006-8993(92)90803-H

Chavez-Noriega, L. E., & Stevens, C. F. (1994). Increased transmitter release at excitatory synapses produced by direct activation of adenylate cyclase in rat hippocampal slices. *Journal of Neuroscience*, *14*, 310–317. https://doi.org/10.1523/JNEUROSCI.14-01-00310.1994

Ferguson, G. D., & Storm, D. R. (2004). Why calcium-stimulated adenylyl cyclases? *Physiology (Bethesda)*, *19*, 271–276. https://doi.org/10.1152/physiol.00010.2004

Fernandes, H. B., Riordan, S., Nomura, T., Remmers, C. L., Kraniotis, S., Marshall, J. J., Kukreja, L., Vassar, R., & Contractor, A. (2015). Epac2 mediates cAMP-dependent potentiation of neurotransmission in the hippocampus. *Journal of Neuroscience*, *35*, 6544–6553. https://doi.org/10.1523/JNEUROSCI.0314-14.2015

Fourcaudot, E., Gambino, F., Humeau, Y., Casassus, G., Shaban, H., Poulain, B., & Luthi, A. (2008). cAMP/PKA signaling and RIM1alpha mediate presynaptic LTP in the lateral amygdala. *Proceedings of the National Academy of Sciences of the United States of America*, *105*, 15130–15135.

Frerking, M., Schmitz, D., Zhou, Q., Johansen, J., & Nicoll, R. A. (2001). Kainate receptors depress excitatory synaptic transmission at CA3–>CA1 synapses in the hippocampus via a direct presynaptic action. *Journal of Neuroscience*, *21*, 2958–2966.

Granseth, B., Odermatt, B., Royle, S. J., & Lagnado, L. (2006). Clathrin-mediated endocytosis is the dominant mechanism of vesicle retrieval at hippocampal synapses. *Neuron*, *51*, 773–786. https://doi.org/10.1016/j.neuron.2006.08.029

Gundlfinger, A., Breustedt, J., Sullivan, D., & Schmitz, D. (2010). Natural spike trains trigger short- and long-lasting dynamics at hippocampal mossy fiber synapses in rodents. *PLoS One*, *5*, e9961. https://doi.org/10.1371/journal.pone.0009961

Gundlfinger, A., Leibold, C., Gebert, K., Moisel, M., Schmitz, D., & Kempter, R. (2007). Differential modulation of short-term synaptic dynamics by long-term potentiation at mouse hippocampal mossy fibre synapses. *Journal of Physiology*, *585*, 853–865. https://doi.org/10.1113/jphysiol.2007.143925

Hashimotodani, Y., Nasrallah, K., Jensen, K. R., Chavez, A. E., Carrera, D., & Castillo, P. E. (2017). LTP at hilar mossy cell-dentate granule cell synapses modulates dentate gyrus output by increasing excitation/inhibition balance. *Neuron*, *95*(928–943), e923. https://doi.org/10.1016/j.neuron.2017.07.028

Herring, B. E., & Nicoll, R. A. (2016). Long-term potentiation: From CaMKII to AMPA receptor trafficking. *Annual Review of Physiology*, *78*, 351–365. https://doi.org/10.1146/annurev-physiol-021014-071753

Huang, Y. Y., & Kandel, E. R. (1998). Postsynaptic induction and PKA-dependent expression of LTP in the lateral amygdala. *Neuron*, *21*, 169–178. https://doi.org/10.1016/S0896-6273(00)80524-3

Huang, Y. Y., Li, X. C., & Kandel, E. R. (1994). cAMP contributes to mossy fiber LTP by initiating both a covalently mediated early phase and macromolecular synthesis-dependent late phase. *Cell*, *79*, 69–79. https://doi.org/10.1016/0092-8674(94)90401-4

Kaeser-Woo, Y. J., Younts, T. J., Yang, X., Zhou, P., Wu, D., Castillo, P. E., & Sudhof, T. C. (2013). Synaptotagmin-12 phosphorylation by cAMP-dependent protein kinase is essential for hippocampal mossy fiber LTP. *Journal of Neuroscience*, *33*, 9769–9780. https://doi.org/10.1523/JNEUROSCI.5814-12.2013

Kamiya, H., Shinozaki, H., & Yamamoto, C. (1996). Activation of metabotropic glutamate receptor type 2/3 suppresses transmission at rat hippocampal mossy fibre synapses. *Journal of Physiology*, *493*(Pt 2), 447–455. https://doi.org/10.1113/jphysiol.1996.sp021395

Kauer, J. A., & Malenka, R. C. (2007). Synaptic plasticity and addiction. *Nature Reviews Neuroscience*, *8*, 844–858. https://doi.org/10.1038/nrn2234

Lachamp, P. M., Liu, Y., & Liu, S. J. (2009). Glutamatergic modulation of cerebellar interneuron activity is mediated by an enhancement of GABA release and requires protein kinase A/RIM1alpha signaling. *Journal of Neuroscience*, *29*, 381–392.

Laurenza, A., Sutkowski, E. M., & Seamon, K. B. (1989). Forskolin: A specific stimulator of adenylyl cyclase or a diterpene with multiple sites of action? *Trends in Pharmacological Sciences*, *10*, 442–447. https://doi.org/10.1016/S0165-6147(89)80008-2

Maximov, A., Shin, O. H., Liu, X., & Sudhof, T. C. (2007). Synaptotagmin-12, a synaptic vesicle phosphoprotein that modulates spontaneous neurotransmitter release. *Journal of Cell Biology*, *176*, 113–124. https://doi.org/10.1083/jcb.200607021

Menegon, A., Bonanomi, D., Albertinazzi, C., Lotti, F., Ferrari, G., Kao, H. T., Benfenati, F., Baldelli, P., & Valtorta, F. (2006). Protein kinase A-mediated synapsin I phosphorylation is a central modulator of Ca2+-dependent synaptic activity. *Journal of Neuroscience*, *26*, 11670–11681. https://doi.org/10.1523/JNEUROSCI.3321-06.2006

Monday, H. R., & Castillo, P. E. (2017). Closing the gap: Long-term presynaptic plasticity in brain function and disease. *Current Opinion in Neurobiology*, *45*, 106–112. https://doi.org/10.1016/j.conb.2017.05.011

Monday, H. R., Younts, T. J., & Castillo, P. E. (2018). Long-term plasticity of neurotransmitter release: Emerging mechanisms and contributions to brain function and disease. *Annual Review of Neuroscience*, *41*, 299–322. https://doi.org/10.1146/annurev-neuro-080317-062155

Nicoll, R. A., & Schmitz, D. (2005). Synaptic plasticity at hippocampal mossy fibre synapses. *Nature Reviews Neuroscience*, *6*, 863–876. https://doi.org/10.1038/nrn1786

Otmakhov, N., Khibnik, L., Otmakhova, N., Carpenter, S., Riahi, S., Asrican, B., & Lisman, J. (2004). Forskolin-induced LTP in the CA1 hippocampal region is NMDA receptor dependent. *Journal of Neurophysiology*, *91*, 1955–1962. https://doi.org/10.1152/jn.00941.2003

Patzke, C., Brockmann, M. M., Dai, J., Gan, K. J., Grauel, M. K., Fenske, P., Liu, Y. U., Acuna, C., Rosenmund, C., & Südhof, T. C. (2019). Neuromodulator signaling bidirectionally controls vesicle numbers in human synapses. *Cell*, *179*(498–513), e422. https://doi.org/10.1016/j.cell.2019.09.011

Rebola, N., Carta, M., & Mulle, C. (2017). Operation and plasticity of hippocampal CA3 circuits: Implications for memory encoding. *Nature Reviews Neuroscience*, *18*, 208–220. https://doi.org/10.1038/nrn.2017.10

Rost, B. R., Breustedt, J., Schoenherr, A., Grosse, G., Ahnert-Hilger, G., & Schmitz, D. (2010). Autaptic cultures of single hippocampal granule cells of mice and rats. *European Journal of Neuroscience*, *32*, 939–947. https://doi.org/10.1111/j.1460-9568.2010.07387.x

Rost, B. R., Schneider, F., Grauel, M. K., Wozny, C., G Bentz, C., Blessing, A., Rosenmund, T., Jentsch, T. J., Schmitz, D., Hegemann, P., & Rosenmund, C. (2015). Optogenetic acidification of synaptic vesicles and lysosomes. *Nature Neuroscience*, *18*, 1845–1852. https://doi.org/10.1038/nn.4161

Rost, B. R., Schneider-Warme, F., Schmitz, D., & Hegemann, P. (2017). Optogenetic tools for subcellular applications in neuroscience. *Neuron*, *96*, 572–603. https://doi.org/10.1016/j.neuron.2017.09.047

Salin, P. A., Malenka, R. C., & Nicoll, R. A. (1996). Cyclic AMP mediates a presynaptic form of LTP at cerebellar parallel fiber synapses. *Neuron*, *16*, 797–803. https://doi.org/10.1016/S0896-6273(00)80099-9

Steuer Costa, W., Yu, S. C., Liewald, J. F., & Gottschalk, A. (2017). Fast cAMP modulation of neurotransmission via neuropeptide signals and vesicle loading. *Current Biology*, *27*, 495–507. https://doi.org/10.1016/j.cub.2016.12.055

Stierl, M., Stumpf, P., Udwari, D. et al (2011). Light modulation of cellular cAMP by a small bacterial photoactivated adenylyl cyclase, bPAC, of the soil bacterium Beggiatoa. *Journal of Biological Chemistry*, *286*, 1181–1188.

Takeuchi, T., Duszkiewicz, A. J., & Morris, R. G. (2014). The synaptic plasticity and memory hypothesis: Encoding, storage and persistence. *Philosophical Transactions of the Royal Society of London. Series B, Biological Sciences*, *369*, 20130288. https://doi.org/10.1098/rstb.2013.0288

Tong, G., Malenka, R. C., & Nicoll, R. A. (1996). Long-term potentiation in cultures of single hippocampal granule cells: A presynaptic form of plasticity. *Neuron*, *16*, 1147–1157. https://doi.org/10.1016/S0896-6273(00)80141-5

Vaden, J. H., Banumurthy, G., Gusarevich, E. S., Overstreet-Wadiche, L., & Wadiche, J. I. (2019). The readily-releasable pool dynamically regulates multivesicular release. *Elife*, *8*. https://doi.org/10.7554/eLife.47434

Vandael, D., Borges-Merjane, C., Zhang, X., & Jonas, P. (2020). Short-term plasticity at hippocampal mossy fiber synapses is induced by natural activity patterns and associated with vesicle pool engram formation. *Neuron*, *107*(509–521), e507. https://doi.org/10.1016/j.neuron.2020.05.013

Weisskopf, M. G., Castillo, P. E., Zalutsky, R. A., & Nicoll, R. A. (1994). Mediation of hippocampal mossy fiber long-term potentiation by cyclic AMP. *Science*, *265*, 1878–1882. https://doi.org/10.1126/science.7916482

Wozny, C., Maier, N., Fidzinski, P., Breustedt, J., Behr, J., & Schmitz, D. (2008). Differential cAMP signaling at hippocampal output synapses. *Journal of Neuroscience*, *28*, 14358–14362. https://doi.org/10.1523/JNEUROSCI.4973-08.2008

Yang, Y., & Calakos, N. (2011). Munc13-1 is required for presynaptic long-term potentiation. *Journal of Neuroscience*, *31*, 12053–12057. https://doi.org/10.1523/JNEUROSCI.2276-11.2011

Zalutsky, R. A., & Nicoll, R. A. (1990). Comparison of two forms of long-term potentiation in single hippocampal neurons. *Science*, *248*, 1619–1624. https://doi.org/10.1126/science.2114039

Zucker, R. S., & Regehr, W. G. (2002). Short-term synaptic plasticity. *Annual Review of Physiology*, *64*, 355–405. https://doi.org/10.1146/annurev.physiol.64.092501.114547

SUPPORTING INFORMATION

Additional supporting information may be found online in the Supporting Information section.

How to cite this article: Oldani S, Moreno-Velasquez L, Faiss L, et al. SynaptoPAC, an optogenetic tool for induction of presynaptic plasticity. *J Neurochem*. 2021;156:324–336. https://doi.org/10.1111/jnc.15210